On the Fundamentals of Bowed-String Dynamics

by M. E. McIntyre and J. Woodhouse

Department of Applied Mathematics and Theoretical Physics, University of Cambridge

Summary

A general class of models of the bowed string is considered. The effect of the bow is idealised in the usual way as a nonlinear friction force f whose ratio to normal bow force F_b depends only on relative velocity at a single point of contact with the string, while the string and its terminations are represented as a linear system with an impulse response $g(t)$ at the bowing point. Thus all the complexities of real strings on real instruments can be allowed for, as long as they are adequately described by linear theory; and all models studied in the past are included as special cases.

A problem of particular interest is the change in vibration waveform and period as F_b is varied. This is found to be in accordance with earlier qualitative predictions, apart from one feature which is familiar from casual observation but which has not previously been explained: as F_b increases beyond a certain critical value, there is a tendency for the oscillation period to increase. This "flattening effect" occurs even for an idealised model string with an exactly harmonic series of natural frequencies, and is caused by a hysteretical difference between the transitions from sticking to slipping and vice versa.

A fast algorithm for solving the relevant equations has been implemented on an interactive computer system which enables the model string to be "played": F_b and the bow velocity can be varied during computation. Thus it is easy to simulate transient motions of musical interest as well as periodic motions. Examples of starting transients are given, together with an example of a "wolf note" in which the behaviour is found to be qualitatively consistent with both the Raman and the Schelleng descriptions. The computer program has been checked by detailed comparison of its results with those of Schumacher obtained in the companion paper [11] by a completely different approach.

Über die Grundlagen der Dynamik gestrichener Saiten

Zusammenfassung

Es wird eine allgemeine Klasse von Modellen einer gestrichenen Saite betrachtet. Die Wirkung des Bogens wird dabei wie üblich idealisiert als nichtlineare Reibungskraft f angenommen, deren Verhältnis zur Bogen-Normalkraft F_b nur von der relativen Geschwindigkeit am Kontaktpunkt mit der Saite abhängt. Die Saite und ihre Enden werden als lineares System mit einer Impulsantwort $g(t)$ am Anstrichpunkt dargestellt. Dadurch können die Vorgänge bei realen Saiten auf realen Instrumenten in ihrer ganzen Komplexität berücksichtigt werden, solange sie angemessen durch eine lineare Theorie beschreibbar sind; alle bisher untersuchten Modelle sind als Spezialfälle enthalten.

Ein besonders interessierendes Problem ist die Änderung der Schwingungsform und der Periode mit F_b. Sie befindet sich in Übereinstimmung mit früheren, qualitativen Aussagen, jedoch mit einer Ausnahme, die aus gelegentlichen Beobachtungen bekannt ist, bisher aber nicht erklärt werden konnte: Wenn F_b über einen bestimmten kritischen Wert hinaus ansteigt, zeigt die Schwingungsperiode die Tendenz, ebenfalls anzusteigen. Diese Tonhöhenerniedrigung tritt sogar bei der idealisierten Modellsaite mit ihrer genau harmonischen Reihe von Eigenfrequenzen auf. Er wird verursacht von einer durch Hysterese bedingten Differenz zwischen den Übergängen vom Haften zum Gleiten und umgekehrt.

Ein schneller Algorithmus zur Lösung der relevanten Gleichungen wurde in ein interaktives Computersystem implementiert, wodurch ein „Spielen" der Modellsaite möglich wurde, d.h. F_b und die Bogengeschwindigkeit konnten während der Berechnung verändert werden. Damit war es möglich, auf einfache Weise sowohl musikalisch interessierende Ausgleichsvorgänge als auch periodische Bewegungen zu simulieren. Es werden Beispiele für Einschwingvorgänge und für einen „Wolfton" angegeben. Für diesen zeigt sich, daß die hier verwendete detaillierte Dynamik sowohl mit den Beschreibungen nach Raman als auch nach Schelleng qualitativ konsistent ist. Das Computerprogramm wurde durch detaillierten Vergleich seiner Resultate mit denen von Schumacher geprüft, die mit einem völlig anderen Ansatz erhalten wurden und die in der begleitenden Arbeit [11] dargestellt sind.

Sur les principes fondamentaux de la dynamique de la corde frottée

Sommaire

On examine tout un ensemble de modèles pour la corde frottée par l'archet. Selon l'usage, l'action de l'archet sera symbolisée par une force de frottement non linéaire f dont la relation avec la force F_b exercée par l'archet normalement à la corde dépend seulement de la vitesse relative au point de contact de l'archet avec la corde, tandis que la corde et ses extrémités sont interprétées comme un système linéaire présentant une réponse impulsionnelle $g(t)$ au point frotté. Ainsi il pourra être tenu compte de toutes les particularités, même les plus complexes, des cordes réelles montées sur des instruments réels pourvu qu'elles puissent être décrites d'une manière adéquate par une théorie linéaire. De plus tous les modèles étudiés dans le passé seront englobés comme cas particuliers.

Un problème spécialement intéressant est celui du changement de forme et de fréquence de la vibration de la corde en fonction de F_b. Ceci s'accorde avec des prédictions qualitatives anciennes, sauf pour la particularité suivante, qui est bien connue grâce à des observations fortuites, mais n'avait pas pu être expliquée jusqu'ici: lorsque F_b dépasse une certaine valeur critique, la période d'oscillation a tendance à augmenter. Cet effet de «bémolisation» apparaît même pour une corde du modèle idéalisé exhibant une série d'harmoniques exacts de fréquences naturelles; il est causé par une différence due à l'hystérésis entre les transitions adhérence-glissement et glissement-adhérence.

Un algorithme rapide pour résoudre les équations du problème a été réalisé pour un système de calculateur conversationnel qui permet en quelque sorte de «jouer» la corde modélisée en faisant varier F_b et la vitesse de l'archet au cours du calcul. Ainsi il est aisé de simuler les mouvements transitoires ou périodiques qui présentent un intérêt musical. On présente des exemples de transitoires d'attaque et un exemple de note «hurlée» dont les détails dynamiques sont qualitativement en bon accord avec les descriptions données par Raman et par Schelleng. Le programme du calculateur a été mis à l'épreuve par comparaison détaillée de ses résultats avec ceux que Schumacher a obtenus dans l'article suivant [11] par une méthode complètement différente.

1. Introduction

In the past, motion of the bowed string has been studied from a number of points of view. Following the early observations of Helmholtz and others [1], [2], the first comprehensive theoretical discussion of the dynamics of the system was given by Raman [3]. He used two models. The first was a kinematic description of a hierarchy of periodic motions, including the basic "Helmholtz motion" [4], which apparently explained most of the complicated behaviour previously observed on the hypothesis that the waveform of string velocity at the bow is a rectangular wave. The second model, which is now usually called the "Raman model", was a dynamical model in which the string was assumed to be an ideal, flexible string terminated in real, frequency-independent mechanical resistances. For the problem in which such a string is "bowed" at a single point dividing the string in a rational ratio $p:q$, the equations describing the motion reduce to a nonlinear difference equation [5], [6] because propagation and reflection are non-dispersive. Thus Raman was able to calculate quite a number of the periodic motions which the model allows, although with hand calculations he was restricted to cases in which $p + q$ was 24 or less.

More recently, Schelleng summarised and re-interpreted some parts of Raman's work in a paper containing much general insight into various aspects of bowed-string motion [7]. In particular Schelleng focussed attention on delineation of the steady-state tolerance range in bowing-parameter space, the region for which musically-useful periodic (or in some cases nearly-periodic [8], [24]) motion may be sustained. He also extended some earlier ideas of Cremer and Lazarus [9], who were the first to consider models of the string in which the travelling Helmholtz "corner" is not perfectly sharp, but instead is somewhat rounded. Their models enabled Cremer and Lazarus to investigate the variation of vibration waveform within the tolerance range. (Raman's model has perfectly sharp corners, and hence no variation.)

One phenomenon, well-known in real bowed strings but not accounted for by any of these previous models, is the "flattening effect". As one presses harder with the bow the note being produced usually goes flat, typically by a small fraction of a semitone. The effect is especially easy to produce when playing with a slow bow in a high position on a thick string, such as the violin G string, and is avoided in normal playing. Here we are talking about a small, continuous flattening of pitch, not the gross change to a raucous, much lower "pitch" characteristic of bowing forces above Schelleng's maximum [7]. In this paper we propose a model which predicts the flattening effect and associates it with a hysteresis phenomenon not previously noted in this context so far as we know.

As well as dealing with this specific effect we try here to unify earlier methods of treatment of the bowed-string problem, in a formulation which encompasses a wide range of possible models and which gives insight into the range of behaviour to be expected from these models. As a result we are led to an efficient method for numerical simulation of general, transient bowed-string motions, with realistic corner-rounding taken into account.

Another suggestion emerging from our formulation is of a new measurement which may be made on instruments, namely the "Green's function" or impulse response at the bowing point, which contains all the information necessary to a simulation of the string motion in any model where the string is bowed at a point. This measurement is a property of an instrument and its strings, and is perhaps the most direct and simple objective measure of the behaviour of the instrument as felt by the player. Thus it might become useful alongside measurements of instrument-body response curves and admittance curves, and studies of eigenmodes of the instrument body, as a tool for seeking physical correlates of the subjective qualities of different instruments. A closely related measure of the behaviour of the instrument (the string input admittance, or Fourier transform of the Green's function) has already been studied experimentally by Hancock [10] and is discussed by Benade [13].

In a companion paper, Schumacher [11] discusses the problem of finding periodic solutions to the models discussed here. His discussion complements the one given here, and the two papers should be read together.

2. General formulation

We now derive the basic equation satisfied by the string motion, when the bow speed v_b and the normal bow force F_b are given. We use the simple idealisation that the bow has zero width, and that the frictional force exerted by the bow on the string depends on relative velocity only. In other words, we assume that a force is applied at one point of the string, the force depending on the velocity of the string at that point according to a known functional dependence $f(v)$ of the type shown in Fig. 1. The entire curve is supposed to scale vertically with F_b. (All previous work has made these assumptions, apart from some qualitative speculation about the effects of finite bow width [3], [5]. It has recently become apparent that some important features of real bowed-string
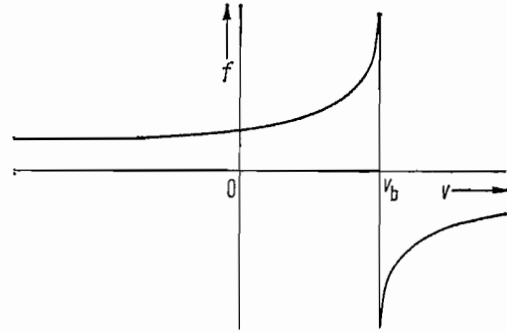

Fig. 1. Friction-curve idealisation. For given bow speed v_b and normal bow force F_b, the friction force f is assumed to be a function of velocity v alone. Steady-state measurements [14] suggest a relationship like that shown.

motion do in fact depend on the finite width of the bow [8], [24], but we ignore such effects here.) When the point (v, f) lies on the very steep, negatively-sloping part of the friction curve we say the string is "sticking" to the bow; otherwise, we say that it is "slipping".

As well as being connected by the friction curve of Fig. 1, the friction force and velocity at the bow are connected by the dynamical behaviour of the string and its terminations, a complicated system which we can regard to good approximation as being linear. If we suppose this linear system to have a causal Green's function or impulse response $g(t)$, we are immediately led to the equation

$$v(t) = \int_0^\infty g(t') f(v(t - t')) \, dt' , \qquad (1)$$

which is a nonlinear integral equation of the Volterra type [12]. (By definition, $g(t') = 0$ for $t' < 0$.) Thus the entire problem is formulated in terms of the motion of the string at the bow. The motion at any other point, for example at the bridge of the instrument, may be obtained from the motion at the bow by a simple convolution of $v(t)$ with the appropriate transfer function.

Eq. (1) embodies one essential ingredient of the philosophy behind the present treatment of the bowed string: as far as possible, we remain in the time domain rather than the frequency domain. It appears that despite the mathematical similarity of our problem to that of sustained oscillations in wind instruments treated so successfully by Benade and others [13] in the frequency domain, the time-domain viewpoint often gives the greater insight for the bowed string. An important reason for this will emerge in the next section.

One general point about eq. (1) should be noted before we pass on: in the actual, physical situation, the $v(t)$ which enters the equation is really the

velocity of the surface of the string, since the friction force is applied tangentially to the surface. Thus in a string of finite diameter having finite torsional characteristic impedance, the Green's function $g(t)$ will contain information about reflecting torsional waves as well as about transverse waves. It is known that this complication cannot be ignored in the real situation [7], [14], but for the purposes of the discussion it will be convenient (and it has hitherto been customary) to begin by imagining that the $g(t)$ of interest is calculated from consideration of transverse motion alone. We shall return to this issue briefly in section 4.

Similarly, the argument of $f(v)$ is not in reality the velocity of the string alone, but that of the string relative to the bow hair. It can easily be shown [11] that this still yields a problem of the form of eq. (1), provided we add to $g(t)$ the impulse response for the elastic behaviour of bow hair and stick, an approximately linear system which has many vibration modes in the frequency range of interest [15]. This contribution to g is numerically small, however [14], [15], and we ignore it entirely for the moment: the models we develop and solve in this article, and all those studied in the past, apply not to a real bow but to a rigid, rosined stick having a single point of contact with the string. (We are currently making observations of the motion of real strings when bowed with just such a rigid stick. These experiments, which as far as we know have not been carried out before, provide the simplest test of our theory as well as giving insight into the differences between sticks and real bows, and it is hoped to report on them in the near future [8].)

As mentioned in the Introduction, the Green's function $g(t)$ (ignoring any contribution from the bow) may be measured directly from a string on a real instrument. It is the velocity response of the string at the supposed bowing point to a force impulse applied there at time $t = 0$. Now a force impulse is hard to realise in practice, but various other forms of applied force may be used, from which the Green's function may be obtained by suitable analysis. The simplest is a step function of force, easily applied by "plucking" the string with a fine thread or wire which breaks when the string is drawn aside [16]. The surface velocity response at the plucked point can be registered by the laser-doppler technique used by Hancock [10]. If the torsional motion is to be ignored, a magnet with suitably-designed pole-pieces can be placed athwart the string and the voltage induced across the ends of the string measured [7], [14]. Since the system we are studying is assumed to be linear,

we obtain the Green's function from this measured response by simple differentiation: a delta function is the time derivative of a step function, and for a linear system whose properties do not change
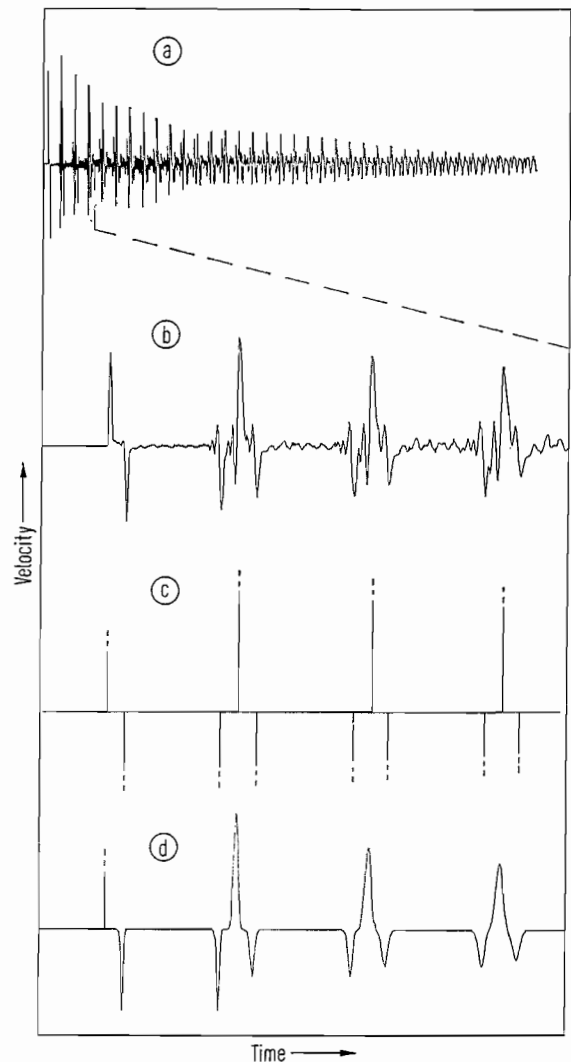

Fig. 2. Green's function $g(t)$ (i.e. velocity response at a point P to a force impulse applied at the same point P): (a) for a cello A string, measured by the magnet technique when P is about 0.14 of a string length from one end; (b) the same, with expanded time scale; (c) for Raman's dynamical model, involving only delta functions (infinitely tall and narrow); (d) for a simple case of the rounded-corner model developed here. The time-scale in (c) and (d) is the same as that of (b), to aid identification of features in (b). Similarly, the position of P for (c) and (d) is the same as for (b). The initial spike of (b) may not be well resolved by our present magnet technique, and is probably narrower in reality.

with time the derivative of the input produces the derivative of the output. Fig. 2a shows an example of a Green's function measured with the magnet technique at a point on the open A string of a cello about 0.14 of a string length from the

bridge. This of course does not show any torsional effects. Fig. 2b shows the detailed structure near $t = 0$.

Green's functions may also be calculated from particular theoretical models of the string. For comparison with Fig. 2b we give in Fig. 2c the Green's function for the Raman model. In this case, $g(t)$ is composed entirely of delta functions, which is one way of seeing why the equation governing the motion is a difference equation. In Fig. 2d we give the corresponding portion of a Green's function for a simple case of the rounded-corner model which we develop in section 5 below (see caption to Fig. 9).

One can compute transient bowed-string motion directly from such a measured or calculated Green's function, integrating eq. (1) forward in time with some particular friction curve $f(v)$. However, it is found that this method is very slow (because the convolution integral to be evaluated grows ever larger as the simulation proceeds), and also it is sensitive to measurement and rounding errors in the Green's function[1]. Thus it is desirable for modelling purposes to supplement the direct use of eq. (1) by a more efficient method, and we describe such a method in the final section. Before that, however, we must show how to resolve an ambiguity which can arise in the solution of eq. (1). The answer will lead inter alia to our explanation of the pitch flattening effect.

3. The small-time behaviour of the Green's function, and hysteresis

The first feature of the Green's function plays a crucial role in the solution of eq. (1). For an ideal string this feature is a positive-going delta function, whose magnitude is half the characteristic admittance (Y, say) of the string. (The numerical value of Y will be modified if we allow for torsional waves or longitudinal bow-hair motion [7], [11], but the argument we are about to use is quite unaffected.) Thus for any reasonable Green's function of a real or model string, we would expect the first feature to be either a delta function or a sharp "spike" of some sort, the area under which we shall denote by $\frac{1}{2} Y$. In either case, it is convenient to consider the effect of this first feature separately, and leave the rest of the Green's function to be accounted for later.

---

[1] More sophisticated methods of determining $g(t)$, e.g. white-noise excitation, might suffer less from the high-frequency errors arising from differentiation of the pluck response [17]. We have not explored any such methods in detail.

If $g(t)$ starts with a delta function of strength $\frac{1}{2} Y$, we can write eq. (1) in the form

$$v(t) = \tfrac{1}{2} Y f(t) + v_{\mathrm{h}}(t) \tag{2}$$

where $f(t)$ is an abbreviation for $f(v(t))$,

$$v_{\mathrm{h}}(t) = \int_0^\infty \hat{g}(t') f(v(t - t')) \, \mathrm{d}t', \tag{3}$$

and

$$g(t) = \tfrac{1}{2} Y \delta(t) + \hat{g}(t),$$

$\hat{g}$ being finite in the neighbourhood of $t = 0$ and zero for $t < 0$. Thus $v_{\mathrm{h}}(t)$ depends only on the past history of the force f at the bow, and is the velocity at the bowing point which would obtain if the bow were suddenly removed. It is due to the net effect of reflections returning from the two ends of the string.

If $g(t)$ starts instead with a spike of finite width described by a function $\frac{1}{2} Y k(t)$ such as that depicted in Fig. 3, and if $\hat{g}$ is redefined by
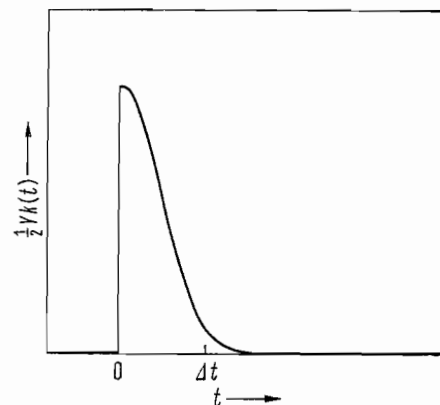
$$g(t) = \tfrac{1}{2} Y k(t) + \hat{g}(t), \tag{4}$$

Fig. 3. A hypothetical example of the initial spike $k(t)$ of a Green's function, on a time-scale expanded still further than in Fig. 2. (The spike width Δt is referred to in Fig. 6.)

with

$$\int_0^\infty k(t') \, \mathrm{d}t' = 1, \tag{5}$$

then

$$v(t) = \tfrac{1}{2} Y \bar{f}(t) + v_{\mathrm{h}}(t) \tag{6}$$

where

$$\bar{f}(t) = \int_0^\infty k(t') f(v(t - t')) \, \mathrm{d}t'. \tag{7}$$

Here $v_{\mathrm{h}}(t)$ is still defined by eq. (3), but with the new definition (4) of $\hat{g}(t)$. Spike shapes different in detail from that in Fig. 3 may arise from particular physical models, as will be discussed in section 4. Note however that $k(t)$ will always jump

discontinuously at $t = 0+$ to a positive value, whether finite or infinite, for otherwise the system would have infinite effective mass.

The delta function case (eq. (2)) is a useful idealisation in practice, and we discuss it first. For given v_h, eq. (2) can be solved for the new values of f and v at time t by the simple graphical
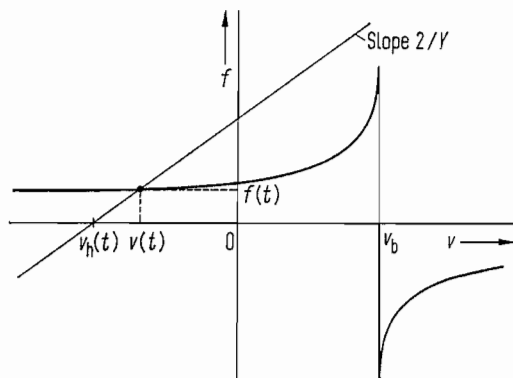

Fig. 4. Graphical construction for determining f and v at time t, given $v_\mathrm{h}(t)$, in the "delta-function case" (see text).

construction shown in Fig. 4, first used by Friedlander [5] and Keller [6]. In Fig. 4, f and v are given by the intersection of the straight line

$$f = 2(v - v_\mathrm{h})/Y$$

with the friction curve. However, for sufficiently large F_b the friction curve can intersect the sloping line in three points rather than one, as shown in Fig. 5, and we have an apparent ambiguity. This
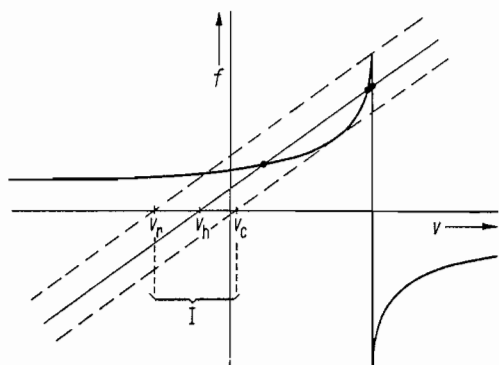

Fig. 5. Friedlander's ambiguity. The solid sloping line now has three intersections with the friction curve instead of one. This happens for any v_h falling in the interval I.

ambiguity, and a possible means of resolving it, was first discussed by Friedlander [5]. Our formalism enables us to generalise Friedlander's discussion, and moreover to show that the correct resolution of the ambiguity is given by a simple hysteresis rule. This leads to an explanation of the flattening effect described in the Introduction. As far as we know, neither the rule nor its musical consequence

has been pointed out before. Friedlander's ambiguity arises from the initial delta function of the Green's function, and we now resolve it by considering eq. (2) as a limiting case of eq. (6) for a wide class of spike shapes $k(t)$.

A numerical example of the behaviour given by eq. (6) is shown in Fig. 6. In this case, $k(t)$ is
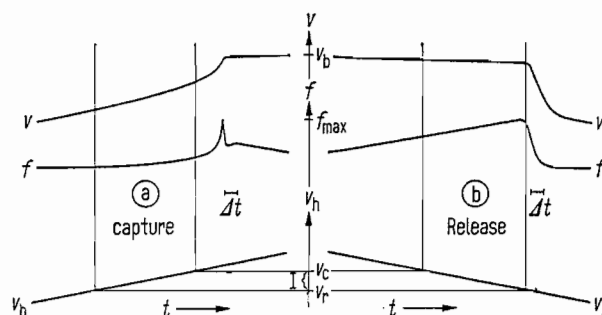

Fig. 6. Numerical simulations of (a) capture and (b) release transients, using the spike function $k(t)$ shown in Fig. 3. The spike width $\varDelta t$ is marked to indicate the time scale. v_h increases in (a) and decreases in (b), through the same range in each case. Note the asymmetry between capture and release: capture takes place when v_h reaches v_c (see Fig. 5), but release is delayed until v_h reaches v_r. The force curves (marked f) give the detailed shape of the "spurs" in Fig. 3 of Schelleng [7], shown here on a vastly expanded time scale.

given by Fig. 3 (shown there expanded in time). Fig. 6a shows velocity v and force f during an idealised "capture" situation, that is to say as v_h increases uniformly across the "ambiguous" interval I of Fig. 5. Fig. 6b shows velocity and force during "release", as v_h decreases at the same uniform rate across I. Note that when v_h enters I, the string simply remains on whichever branch of the friction curve (slipping or sticking) corresponds to its previous state; v and f follow v_h more or less as the graphical construction for the delta-function case indicates (Fig. 4) as long as v_h remains within I. The rapid transition from slipping to sticking, or vice versa, does not take place until v_h reaches the far end of the interval I. The time for the transition scales with the width $\varDelta t$ of the spike $k(t)$.

Computations for various other spike shapes $k(t)$ reveal the same general pattern of behaviour. To summarise:

Slipping persists until v_h has increased as far as v_c; then capture occurs (v rapidly traverses the portion of the friction curve shown dashed in Fig. 7a, and reaches v_b). Sticking persists until v_h has decreased as far as v_r; then release occurs (v rapidly traverses the portion of the friction curve shown dashed in Fig. 7b, and reaches v_slip).
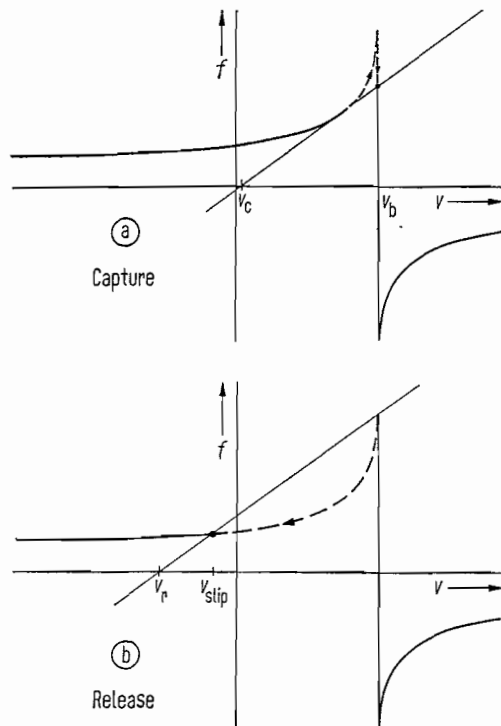
Fig. 7. The hysteresis rule. During capture (a) and release (b), the dashed portions of the friction curves are traversed in a time of order the width Δt of the initial spike $k(t)$ (and instantaneously in the limit in which the spike becomes a delta function).

.Since $v_r \neq v_c$ (except for values of F_b below some rather low value F_{crit}, say), this behaviour pattern involves a kind of hysteresis, an essential difference between capture and release.

The rapidity with which the dashed portions are traversed is the greater, the narrower the spike $k(t)$. In the limit in which the spike tends to a delta function, the dashed portions of the friction curve in Fig. 7 are traversed instantaneously. With the word "rapidly" replaced by "instantaneously", the indented statement above constitutes the hysteresis rule for resolving Friedlander's ambiguity when solving eq. (2). (Note that the term "hysteresis" as used here has nothing to do with the possibility, discussed later, of hysteretical effects in the friction characteristic itself — i.e. departures from the present idealisation that f is a function of v alone.)

Solving eq. (6) for special cases of $k(t)$ can never entirely remove the doubt that there might still be some other model producing quite different behaviour. However it will next be shown that a large class of spike functions $k(t)$ produce essentially the same behaviour as that just described. This class, essentially those $k(t)$ which decrease monotonically for $t > 0$, is specified precisely in Appendix A (below eq. (A.13)). It includes all

reasonable physical models of which we are aware. The result ensures that all these models, in the limit in which the spike $k(t)$ becomes shorter and taller while preserving its area, will give the same hysteresis rule for use with eq. (2). We conclude that the delta-function model, together with the hysteresis rule, provides a physically reasonable idealisation of virtually any model.

To establish the general result we must demonstrate two things, for all $k(t)$ in the class considered. The first is the persistence of the current state of sticking or slipping when v_h enters the interval I. The second is that a transition to the other possible state takes place, on the time-scale Δt of the spike width, when v_h emerges from I. We can make both these aspects of the hysteresis rule immediately plausible by generalising a linear stability result mentioned by Schelleng [7]. The generalised stability result, proved in Appendix A, is also a useful preliminary to a more rigorous discussion given in Appendix B. The linear stability theory concerns the behaviour of $v(t)$ when v_h is held constant and the friction curve of Fig. 1 is locally replaced by a linear function

$$f(v) = Av + B. \qquad (8)$$

As Schelleng remarked, and as we show in Appendix A, the corresponding steady-state solution

$$v = (v_h + \tfrac{1}{2} Y B)/(1 - \tfrac{1}{2} Y A) \qquad (9)$$

is stable if and only if the slope A of this linear "friction curve" satisfies

$$A < 2/Y. \qquad (10)$$

Note that because the solution (9) represents a steady state, it is given by precisely the graphical construction of Fig. 4, just as in the delta-function case. The stability criterion (10) holds for any $k(t)$ in the class considered. Together with the obvious fact that the characteristic times of disturbances to the steady state scale with Δt, it makes plausible the persistence of the current state of sticking or slipping while the slope of the friction curve is less than $2/Y$, provided $v_h(t)$ varies slowly compared with the (very fast) time-scale Δt. (Of course, the sticking portion of the friction curve is taken to have a very large negative slope, not a positive one, since sticking is observed to be a statically stable state.) The instability of the solution (9) for slopes A greater than $2/Y$ also makes it plausible that v will never, in practice, remain near the middle one of the three intersections in Fig. 5 for longer than a time of order Δt ([7], § IIK]).

The main mathematical question left open by the linear theory is whether finite-amplitude dis-

turbances and the actual nonlinear friction curve $f(v)$ admit some other kind of behaviour, such as persistence of finite-amplitude oscillations induced at capture or release. Such possibilities are, however, eliminated by the discussion given in Appendix B, where it is shown that whenever v_h takes on a constant value lying outside I the single intersection then represents a steady solution which is stable to disturbances of any amplitude.

4. The small-time behaviour for particular physical models

Now that we have seen how a wide class of initial spikes $k(t)$ produce essentially the same behaviour, it is apparent that no very detailed study of this aspect of particular physical models is justified (unless we are interested in extraordinarily fine detail in the bowed-string waveform). However, it is worth looking briefly at the most obvious physical models, if only to verify that they fall within the assumed class of k's.

Conceptually, the simplest physical model which produces a spike of finite width rather than a delta-function is an ideal string having a small mass m concentrated at the bowing point. This is the model suggested by Friedlander [5] to circumvent the ambiguity which he first pointed out, and he argued that it might also model some aspects of the finite length of string in contact with a real bow. However, he did not examine its consequences in any detail. The $k(t)$ resulting from such a model is readily seen to be

$$k(t) = (2/Ym)\,e^{-2t/Ym} \quad \text{for} \quad t > 0, \tag{11}$$

and is illustrated in Fig. 8a. This model has the easily demonstrated property that in the transition from slipping to sticking, and vice versa, the approach to the new state is monotonic. This contrasts with the weakly oscillatory behaviour at capture already illustrated in Fig. 6a for a different spike shape.

The next model which one might think of using is the classical, slightly stiff string (e.g. Rayleigh [19], § 188). We illustrate the behaviour of this model by the simple example of the Green's function at the midpoint of a stiff string with hinged ends:

$$g(t) \propto \sum \cos(\omega_n t) \quad \text{with}$$
$$\omega_n{}^2 = n^2 (1 + \gamma n^2) \tag{12}$$

where γ is a small positive parameter and the sum is taken over odd integers n from 1 to infinity. It turns out that this is far from being a desirable Green's function to study: the series of eq. (12)
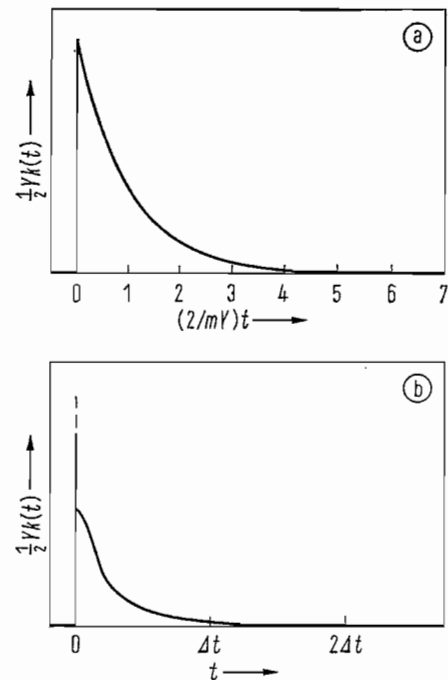

Fig. 8. Spike functions $k(t)$ for two particular physical models: (a) an ideal string with a point mass at the bow; (b) a slightly stiff string, with the high-frequency behaviour modified according to Timoshenko beam theory. In case (b) there is a "residual delta-function" at $t = 0$, accounting for roughly a third of the total area in this particular case. The time interval Δt marked in (b) corresponds to $1/100$ of a fundamental period of the string, for a case in which the "anharmonicity parameter" $n_{\min}$ of Schelleng [7] is equal to 16 (thus corresponding to Schelleng's measurement of a violin aluminium-on-gut D string).

is known to represent an extremely pathological function [20]. This undesirable mathematical behaviour is not special to mid-point bowing, and results from the incorrectness of the classical stiff-string equation at wavelengths comparable to the string diameter or smaller. Thus some modification of the high-frequency terms in the series (12) is necessary, and different detailed models result from different modifications. A model in which Timoshenko beam theory [21] is used to suggest a more physically reasonable asymptotic form of the terms in series (12) yields the function $k(t)$ shown in Fig. 8b. As frequency tends to infinity in this model, the phase speed of waves tends to a constant value roughly an order of magnitude larger than low-frequency transverse-wave speeds, for parameter values appropriate to practical strings.

One feature of Fig. 8b should be noted: because of the model dispersion property just mentioned, $k(t)$ has a delta-function at $t = 0$ on top of a finite-width spike. So in this case Friedlander's ambiguity comes back, but at larger values of F_b than before because the strength of the "residual delta func-

tion" is less than the total area of unity. We presume that a similar hysteresis rule will apply, but this time its justification would have to be sought outside the basic model as formulated in section 2, a problem which would require us to go more deeply into the underlying physics. Fortunately the resolution of this question (which we do not attempt here) in no way affects the hysteresis rule of section 3, since the class of $k(t)$'s for which the stability analysis of Appendices A and B holds includes cases with residual delta-functions like that in Fig. 8b.

The residual delta-function also occurs when we extend our interpretation of string motion to include torsional string motion and bow-hair motion as well as transverse string motion. As Schumacher demonstrates [11], these two effects both enter the problem in the same way. Simple models of either are likely to produce extra delta-function contributions to the total $k(t)$. From published measurements we might expect the torsional effect to dominate, and in the presence of bending stiffness to produce a $k(t)$ qualitatively like that of Fig. 8b, with a residual delta-function whose area depends on the torsional-to-transverse admittance ratio [7].

We will not discuss this issue in any further detail, but it is worth mentioning the two most obvious aspects of the basic physical model which would need to be re-examined in order to resolve the ambiguity due to a residual delta-function. The first is the assumption of a single point of contact between the bow (or stick) and the string. This is obviously an idealisation which will eventually break down when very short length-scales are considered. The second aspect is the "friction curve idealisation", in which we have assumed that the function $f(v)$ is really independent of other factors such as "memory" effects. To describe the motion in very fine detail one would no doubt have to take account of the tribology of the rosined bow-string contact.

A direct experimental test of the friction-curve idealisation deserves the attention of experimenters in any case, since the only existing measurements [14] were taken at constant relative velocity. For all we know, rosin tribology may significantly modify the grosser features of bowed-string behaviour as well. For instance if departures from the friction-curve idealisation involve additional hysteretical effects such as reported for materials other than rosin [18], these would probably tend to add to the hysteretic effect described above. A promising experimental technique for investigating rosin tribology is essentially that

used in ref. [18], involving analysis of the motion of an audio-frequency "Froude's pendulum" excited by a bow. Another promising technique is suggested in the second reference of [8].

5. The remainder of the Green's function, and an efficient method for numerical implementation of bowed-string models with realistic "corner-rounding"

Now that we know how to deal with Friedlander's ambiguity, we can return to a discussion of the use of eqs. (2) and (3) for the simulation of transient as well as periodic motions of the string. Having discussed the small-time behaviour of the Green's function, we now look at the next features. Referring back to Fig. 2b we see that, after the initial spike, there follows a pair of inverted pulses with different time delays. These are, of course, the reflections of the initial pulse from the two ends of the string. During their journeys the reflected pulses are modified in various ways, both by effects internal to the string and by the reflection properties of the terminations. The pulses become increasingly rounded, and rapidly develop dispersive precursors because of the anharmonicity due to string bending stiffness; the gentler oscillations visible between the two first reflections are due mainly to bridge motion.

If, as we have assumed, the string and its terminations behave linearly, we can represent the total modification of the returning pulses by convolution of the velocity waveforms sent out from the bow with a suitable pair of transfer functions, one for reflection from each end of the string. These two "corner-rounding functions", as we shall somewhat loosely call them, can in principle be determined directly from analysis of measured Green's functions such as that shown in Fig. 2b. In an idealised model using a string with harmonic overtones, but with damping smoothly increasing with frequency, the corner-rounding functions can be simple, symmetrical humps. Fig. 2d shows the Green's function for just such a model, and here the corner-rounding functions have almost precisely the shapes of the first two inverted spikes.

Once we know the initial behaviour of $g(t)$ and the two corner-rounding functions for the two sections of the string, we can calculate the rest of the Green's function. All succeeding events are simply further reflections of the original pulse as it travels back and forth along the string, the pulses in $g(t)$ becoming ever more rounded. Each reflection can be derived from the previous one by con-

volution with the appropriate corner-rounding function. It follows that if we wish to simulate transient motion of the bowed string by solving eqs. (2) and (3) numerically, we need not store the entire Green's function and past history of $v(t)$ for hundreds of string periods and perform huge convolution integrals at each time step. Instead we need only store the velocity waves $v_L(t)$ and $v_R(t)$ travelling away from the bow to the left and right respectively, and convolve the retarded waves $v_L(t - t_L)$ and $v_R(t - t_R)$ with the appropriate corner-rounding functions and add the results to give $v_h(t)$ at each time step, where t_L and t_R are the reflection times for the two sections of the string. Thus the "history" of the motion need only be stored for a short time, namely t_L or t_R plus the decay time of the corresponding corner-rounding function, rather than the decay time of the whole Green's function.

This amounts to the procedure outlined by Cremer [9], with two additional features. First, whereas Cremer neglected the "secondary waves" produced by partial reflection at the bow (as part of the corner-sharpening process due to interaction of rounded corners with the bow-string contact), our procedure automatically keeps track of all such secondary waves and follows the evolution of the complete string motion. Second, we introduce the hysteresis rule of section 3, whenever F_b exceeds the value F_{crit} for which Friedlander's ambiguity arises. A computer program has been written to implement the procedure, and its detailed correctness has been verified by closely comparing results with those of Schumacher [11], who has computed periodic solutions to some of the same models by a quite different approach. For this comparison, our program was left to run for many hundreds of string periods to settle down to a precisely periodic solution.

The results show a significant consequence of the hysteresis behaviour described in the previous section. If we set up an approximation to the classical "Helmholtz motion" in our model string, it is not hard to see that the asymmetry between capture and release at the bow imposes a net delay in the round-trip time of the Helmholtz corner. In other words, the note plays flat, other things being equal. The kinematical essentials of the flattening process have been explained at greater length in a previous article [8] using a graphical representation like that of Cremer and Lazarus [9]. The flattening increases with the amount of hysteresis, which in turn increases with normal bow force F_b and decreases with increasing bow speed. Also, the amount of flattening evidently

scales with the breadth of the humps in the corner-rounding functions. All these features are broadly in accordance with observation: flattening is greatest at large F_b and small bow speed, and when playing in high positions on thick strings.

Computed examples were given in reference [8], and in Fig. 9 we reproduce three of these. Further examples are given in Fig. 5 of the companion paper by Schumacher [11]. Both sets show how the velocity waveforms $v(t)$ and playing frequencies vary because of hysteresis, corner-sharpening, and secondary-wave generation, as F_b is varied. Schumacher's examples incorporate effects of string anharmonicity, as well as torsional vibration modes
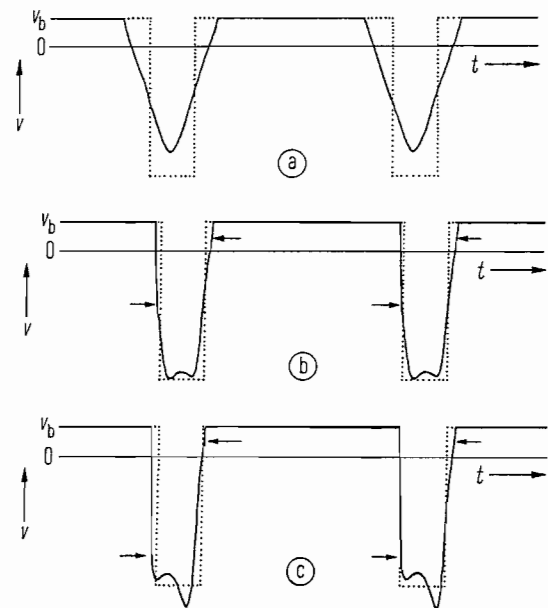

Fig. 9. Typical velocity waveforms at the bow from computer solutions of the corner-rounding model described in the text, for a model string with harmonic overtones, whose Q's decrease as frequency increases. F_b varies from rather low in (a) to near maximum in (c); see below. The dotted curves in each case denote the ideal "Helmholtz" waveforms: the flattening effect is visible in (b) and (c), the frequency having been lowered by about 1.5% and 3% respectively in these two solutions. The corner-rounding function used for these runs was a symmetrical, Gaussian hump $\exp(-t^2/t_c^2)$, so that the low-F_b solution (a), which is non-hysteretic, plays at the natural pitch of the string and gives a symmetrical velocity waveform. In (b) and (c) arrows indicate the discontinuous velocity jumps across the dashed portions of the friction curve in Fig. 7. The corner-rounding time-scale t_c was $\sqrt{3}/128$ of a fundamental period, giving a Q of about 300 for the fundamental string mode. (Fig. 2d has the same corner-rounding function, but with t_c smaller by a factor $(2/3)^{1/2}$.) The friction curve used here had a coefficient of sticking friction of 1.0 (corresponding to the tip of the curve), and a coefficient of sliding friction of 0.2 at the nominal "Helmholtz" slipping velocity. In units such that $1/2\ \Gamma = 1$, the three bow forces used were $0.4\ v_b$, $3.0\ v_b$ and $5.0\ v_b$. There are 128 time steps per Helmholtz period in each case. The bow is 3/16 of the way along the string.
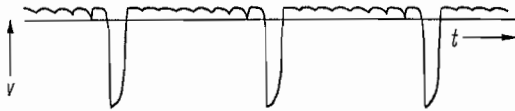
Fig. 10. Waveform of string-centre velocity at the bow in the simplest model which allows for torsional string motion. Torsional waves are assumed, somewhat unrealistically, to be totally absorbed by the string terminations; and the transverse overtones are harmonic as before. The torsional and transverse string admittances are in the ratio 0.4. F_b is large enough to cause the hysteresis effect described in § 3. The difference in size of the ripples near the beginning and end of each sticking epoch recalls an experimental observation of Schelleng [7], and is another manifestation of the hysteresis effect.

of the string. Fig. 9, by contrast, corresponds to a much simpler Green's function like that of Fig. 2d. In Fig. 10 we give a further example, chosen to exhibit clearly the pattern of ripples due to secondary waves pointed out by Schelleng [7] (vide § II J). In this example torsional motion of the string was allowed, and the velocity of the string centre plotted instead of $v(t)$. Note the hysteresis-induced asymmetry in the ripple pattern.

The present approach also allows us to simulate various transient phenomena. We illustrate first with a simple starting transient. Fig. 11a shows velocity at the bow during a simulated "martelé". (The simulation has been implemented on a mini-computer in such a way that the playing parameters of bow force and bow speed may be changed at
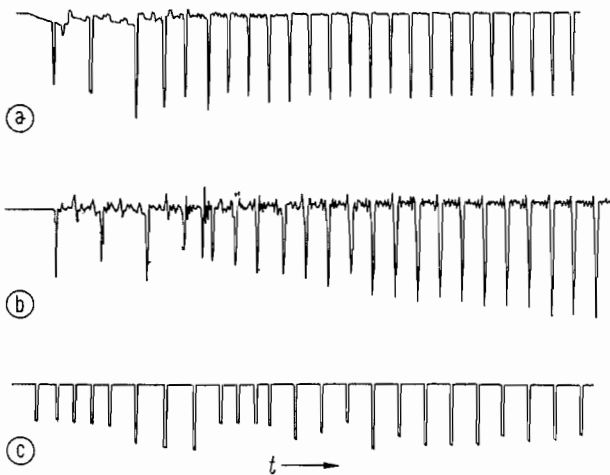
will from the computer keyboard during the simulation: the model can be "played".) For comparison, an observed martelé transient is shown on a comparable time-scale in Fig. 11b. This was obtained using a (somewhat crude) magnetic transducer of the kind previously described, on a low B flat played on the G string of a violin (of no particular pedigree). Note that the observed and simulated transients, while being obviously different in detail, occupy similar times. It may well be that with an experimental facility for accurately measuring bow speeds and normal bow forces (as well as friction curves) during playing, one could produce a better-matched pair of real and theoretical results; but no two real transients are identical under practical playing conditions. In addition, the player of the violin was much more accomplished at his art than the "player" of the computer program! In Fig. 11c, a final example of a starting transient is shown, this time from the Raman model. This example, with no corner-rounding effects, is visibly less realistic than Fig. 11a.

Another transient phenomenon of interest is the "wolf note". By using a corner-rounding function for the "bridge" end of the string of the kind illustrated in Fig. 12, we can simulate the effect
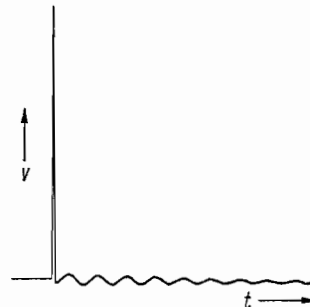

(a)

(b)

(c)

Fig. 11. Simulated and observed "martelé" starting transients (in which the initial condition is one of sticking, and v_b is rapidly increased from zero while F_b is decreased from a high value). (a) Simulated, with the same simple model that produced Fig. 10 but with a torsional-to-transverse admittance ratio of 0.2 in this case; (b) measured with the magnet technique from a violin G string stopped a minor third up and played by a professional violinist; (c) simulated, with the Raman model (in which no corner-rounding, nor torsional motion, is allowed). The magnet used in (b) unfortunately has rather broad pole-pieces, and thus sees some string motion away from the bow.

Fig. 12. "Corner-rounding" function of the type needed for wolf-note simulation. The Q of the decaying sinusoidal oscillation (simulating the effect of a body mode) is 30 here. The initial hump (which is in fact a smooth, Gaussian function) gives frequency-dependent damping of string modes exactly as before. The ratio of characteristic string impedance to $(SM)^{1/2}$, where S and M are effective stiffness and mass at the bridge [23], is here 0.05. This ratio is unrealistically large, but was chosen to make the decaying oscillation clearly visible in the picture. Torsional motion is not allowed for.

of a strong resonance of the instrument body. When the playing frequency is sufficiently close to the frequency of this resonance, we can obtain, with suitable playing parameters [23], a waveform such as that shown in Fig. 13. Here we see a classical wolf note of the kind discussed at length by Raman [27] and Schelleng [23]. The details, including the phase relations between string and
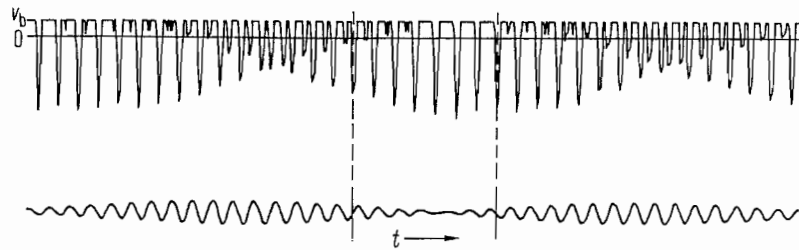
Fig. 13. The simplest kind of wolf note, simulated with one corner-rounding function replaced by a function similar to that of Fig. 12, but with a body Q of 50 and a more realistic string-to-body impedance ratio $Y^{-1}(SM)^{-1/2} = 0.005$; cf. Fig. 9 of Schelleng [23]. The upper trace is string velocity $v(t)$ at the bow, showing the onset of double slip and approximate phase-reversal at the beginning of each wolf cycle. The lower trace is velocity of the bridge, with the vertical scale exaggerated by a factor 2. The phase relations, indicated by the vertical dashed lines, are roughly in accordance with the discussions of Raman and Schelleng [23], [24], [27]. All conditions are the same as in Fig. 9, except for the decaying oscillation in one of the two corner-rounding functions, and a bow force $F_b = 0.8\, v_b$. The main pulses are shaped very like those in Fig. 9a. (Very small scale irregularities in individual pulse shapes are artifacts of the computer graphics. The pulse shapes, and the dashed lines indicating phase relationships, were determined from a much higher-resolution plot.)

body motion, are qualitatively as would be expected from the arguments given by those authors (see [24], section 8), except that the phase change between wolf cycles is somewhat less than 180° (just as observed in an experiment by Firth [28], Fig. 7) because the second slip tends to be triggered early by secondary waves.

6. Concluding remarks

It appears that the model of bowed-string motion elaborated here is capable of plausible behaviour. However, it is not the last word on the subject. We already know that finite bow width is important for a correct description of the noise component, or quasi-random departure from periodicity, of real bowed-string motions [8], [24]. Also, more experimental data is needed to determine relevant properties of real strings on real instruments. A particularly crucial area of present ignorance is the damping and reflection properties of torsional waves in strings. The present class of models can easily simulate their effects, and they are certainly important to the detailed waveform. Once the experimental data are available, a quantitative comparison of computed velocity waveforms with experiment might be appropriate. This in turn might show the extent to which the theory must be modified to take account of longitudinal waves and other nonlinearities of the string, and the complexities in the behaviour of the body and string which contribute to the shape of experimentally measured corner-rounding functions [22]. The laser-doppler technique recently proposed by Hancock [10] for precise observation of motion at the string surface holds promise for obtaining the needed data. We hope to be able to report further progress on this problem before long.

We are at present also investigating the application of the ideas of this article to other frictionally maintained oscillators such as Froude's pendulum [18]. In addition to their importance in other engineering contexts, such oscillators provide a powerful experimental tool for investigating friction curves, and indeed the friction-curve idealisation itself.

Appendix A
Schelleng's criterion for stability local to the bowing point

We consider the linear problem in which in place of a friction curve like that of Fig. 1, we use a linear function

$$f = Av + B. \tag{A.1}$$

This is the simplest problem in which to examine the effect of different functions $k(t)$. We impose a disturbance on the system by making v_h change

from one steady value to another, specifically

$$v_{\mathrm{h}}(t) = \begin{cases} 1, & t < 0 \\ 0, & t > T > 0 \end{cases} \qquad (A.2)$$

with the understanding that, for $t < 0$, the system is in the steady state

$$v = (1 + \tfrac{1}{2} YB)/(1 - \tfrac{1}{2} YA),$$
$$f = (A + B)/(1 - \tfrac{1}{2} YA) \qquad (A.3)$$

(which is evidently a possible solution of eqs. (A.1) and (6)). For $t > T$ we then ask whether or not the system approaches the possible steady state

$$v = \tfrac{1}{2} YB/(1 - \tfrac{1}{2} YA),$$
$$f = B/(1 - \tfrac{1}{2} YA). \qquad (A.4)$$

The system is stable if and only if it tends to this new steady state for all functions $v_{\mathrm{h}}(t)$ satisfying eqs. (A.2).
Write

$$\Delta v = v - \tfrac{1}{2} YB/(1 - \tfrac{1}{2} YA),$$
$$\Delta f = f - B/(1 - \tfrac{1}{2} YA) \qquad (A.5)$$

and choose units in which

$$\tfrac{1}{2} Y = 1 \qquad (A.6)$$

for convenience. Then eq. (6) becomes

$$\Delta v(t) = A \int_{-\infty}^{\infty} k(t')\, \Delta v(t - t')\, \mathrm{d}t' + $$
$$+ h(t) + p(t) \qquad (A.7)$$

where $k(t') = 0$ for $t' < 0$,

$$h(t) = \begin{cases} 1, & t < 0 \\ 0, & t > 0 \end{cases} \qquad (A.8)$$

and

$$p(t) = 0, \quad t \notin [0, T]. \qquad (A.9)$$

We now take the Fourier transform of eq. (A.7), and write $V(\omega)$ and $K(\omega)$ for the Fourier transforms of $\Delta v(t)$ and $k(t)$ respectively, with the convention

$$2 \pi K(\omega) = \int_{-\infty}^{\infty} k(t)\, \mathrm{e}^{-\mathrm{i}\omega t}\, \mathrm{d}t. \qquad (A.10)$$

Then eq. (A.7) gives

$$V(\omega) = 2 \pi A K(\omega)\, V(\omega) + $$
$$+ \mathrm{i}/2 \pi \omega + P(\omega) \qquad (A.11)$$

where $P(\omega)$, the Fourier transform of $p(t)$, is an entire (non-singular) function of ω. Therefore

$$V(\omega) = [P(\omega) + $$
$$+ \mathrm{i}/2 \pi \omega]/[1 - 2 \pi A K(\omega)]. \qquad (A.12)$$

This transform is to be inverted using a contour which passes above the pole at the origin but below

all other poles of $V(\omega)$, because to satisfy the condition (A.3) for $t < 0$ we need to be able to complete the contour in the lower half-plane, and in the process enclose only the pole at the origin. It now follows by standard contour-integral techniques that the steady state represented by eq. (A.4) is stable if and only if $V(\omega)$ has no poles in the lower half-plane or on the real axis (excepting the pole at $\omega = 0$), i.e. if and only if

$$2 \pi K(\omega) = 1/A \qquad (A.13)$$

is satisfied only at points where $\mathrm{Im}(\omega) > 0$. We denote the lower half-plane by L, and L plus the real axis by $\overline{L}$.

Attention is restricted to spike functions $k(t)$ which are non-negative and non-increasing for $t > 0$ (as well as zero for $t < 0$). We permit jump discontinuities in $k(t)$, but assume that at least some of the decrease of k with t is continuous: specifically, there is some interval over which k has a finite, negative slope $k'(t)$. At $t = 0$, a positive delta function contribution is permitted, as in the example of Fig. 8b. Now, writing $\omega = \alpha + \mathrm{i}\beta$, we have from eq. (A.10)

$$\mathrm{Re}[2 \pi K(\omega)] = \int_{0-}^{\infty} k(t)\, \mathrm{e}^{\beta t} \cos \alpha t\, \mathrm{d}t \qquad (A.14a)$$

and

$$\mathrm{Im}[2 \pi K(\omega)] = - \int_{0}^{\infty} k(t)\, \mathrm{e}^{\beta t} \sin \alpha t\, \mathrm{d}t. \qquad (A.14b)$$

Thus for $\beta \leq 0$ (i.e. $\omega \in \overline{L}$), and when $k(t)$ is restricted as above, it is clear that $k(t)\, \mathrm{e}^{\beta t}$ is restricted in the same way and therefore that

$$\mathrm{Im}[K(\omega)] \{\gtreqqless\} 0 \quad \text{according as}$$
$$\alpha \{\lesseqqgtr\} 0, \qquad (A.15)$$

since contributions from successive cycles of $\sin \alpha t$ to $\int \ldots \mathrm{d}t$ have the same sign as α, and not all such contributions can vanish. So the imaginary part of eq. (A.13) (i.e. $\mathrm{Im}[K(\omega)] = 0$) can be satisfied by $\omega \in \overline{L}$ only for $\alpha = 0$. But then the real part of eq. (A.13) requires

$$\int_{0-}^{\infty} k(t)\, \mathrm{e}^{\beta t}\, \mathrm{d}t = 1/A \qquad (A.16)$$

with $\beta \leq 0$. Now

$$\int k(t)\, \mathrm{e}^{\beta t}\, \mathrm{d}t > 0$$

clearly (cf. eq. (5)). Also with $\beta \leq 0$ and $k(t)$ as above,

$$\int_{0-}^{\infty} k(t)\, \mathrm{e}^{\beta t}\, \mathrm{d}t \leq \int_{0-}^{\infty} k(t)\, \mathrm{d}t = 1, \qquad (A.17)$$

by eq. (5), with equality when $\beta = 0$. So eq. (A.16) can be satisfied for some $\omega \in \overline{L}$ if and only if $1/A$ lies between 0 and 1: i.e. when $A \geq 1$. Thus the

steady state for $t > 0$ is stable if and only if $A < 1$ (in the units of eq. (A.6)), or in dimensional terms, if and only if

$$A < 2/Y. \qquad (A.18)$$

This is the result stated by Schelleng ([7], § II K]); our analysis shows that it holds good for a rather general class of spike functions $k(t)$.

The analysis in Appendix B will show that inequality (A.18) is sufficient for stability of the steady state in the nonlinear case also, if A is reinterpreted as the local slope of the friction curve.

Appendix B
Finite-amplitude local stability with a nonlinear friction curve

The problem and notation are the same as in Appendix A, except that we now assume a non-linear friction curve $f(v)$ like that of Fig. 1. The only restriction is the physically reasonable one that the slope be everywhere finite: in particular the negative slope of the steep "sticking" portion can be arbitrarily large in magnitude, but it is not allowed to be infinite anywhere. In place of eq. (A.2) we shall assume that, as time goes on, v_h approaches a constant value v_{h0} such that the sloping line $f = v - v_{h0}$ (in the dimensionless units of eq. (A.6)) has only one intersection (v_0, f_0) with the friction curve $f(v)$, and

$$f'(v_0) < 1.$$

We can then employ a standard result from control theory to show that the steady state (v_0, f_0) is stable to disturbances of any magnitude, and therefore must be approached as time goes on. An immediate corollary is that, even when there are three intersections (i.e. when $v_h \in I$ of Fig. 5), the outer two intersections are stable to any disturbance whose peak excursion (in v) toward the middle, unstable intersection does not reach as far as that intersection. This indicates how large a disturbance is needed before there is any possibility of upsetting the persistence of sticking or slipping as v_h enters the "ambiguous" interval I, and helps explain why this never happened in any of the numerical computations mentioned in section 3.

The permitted class of spike functions $k(t)$ is the same as before (see the statements preceding eq. (A.14)). We shall make use of some of the implied properties of the transform

$$K(\omega) = K(\alpha + i\beta)$$

when $\beta = 0$ and $\alpha \geq 0$, starting with the facts, obvious when we recall eqs. (A.14) and (A.17),

that

$$2\pi K(0) = 1, \qquad (B.1)$$

$$-1 \leqq \text{Re}[2\pi K(\alpha)] \leqq 1 \qquad (B.2)$$

(this follows at once on setting $\beta = 0$ in eq. (A.14a) and using $|\cos \alpha t| \leqq 1$). Defining $H(\alpha)$ by

$$2\pi K(\alpha) = \varepsilon + H(\alpha), \qquad (B.3)$$

where ε is a real constant satisfying $0 \leqq \varepsilon < 1$, which is equal to the strength of any "residual delta-function" which may contribute to $k(t)$ at $t = 0$, we see from relation (B.2) that the real part of $H(\alpha)$ satisfies

$$-1 - \varepsilon \leqq \text{Re}[H(\alpha)] \leqq 1 - \varepsilon. \qquad (B.4)$$

Further, by applying Riemann's lemma [25] to the integral representation

$$\int_{0+}^{\infty} k(t) e^{-i\alpha t} dt$$

of $H(\alpha)$, and noting that k is non-increasing and $\int k \, dt$ finite, we deduce that there is a positive constant C such that

$$|H(\alpha)| \leqq C \min(1, \alpha^{-1}) \qquad (B.5)$$

for all $\alpha \geqq 0$. Finally, it can be shown at some length that

$$\text{Im}[2\pi K(\alpha)] \leqq -D \min(\alpha, \alpha^{-1}) \qquad (B.6)$$

for all $\alpha \geqq 0$, where D is a positive constant, for any given k in the class under consideration. This is a stronger version of the lower inequality of relation (A.15) and, as with that inequality, is a consequence of the hypothesis that $k(t)$ has a finite, negative slope over some non-vanishing time interval. The proof of inequality (B.6) is straightforward and the details are omitted. Its essence is to note first that, by hypothesis, $k'(t)$ is less than some negative constant for all t in some finite interval J; second, that the contribution to the integral (A.14b) from each cycle of $\sin \alpha t$ is non-positive; and finally that the cycle or cycles which intersect J give negative contributions, when $\alpha > 0$, whose magnitude is at least proportional to α for small α, and to α^{-1} for large α. (For large α, each cycle falling within J contributes α^{-2} times a (negative) quantity of order unity; and the number of such cycles is proportional to α.)

We now transform eq. (6) by writing

$$v_h - v_{h0} = \Delta v_h, \quad v - v_0 = \Delta v, \qquad (B.7)$$

and

$$f(v) - f_0 = \theta \Delta v - \varphi(\Delta v) \qquad (B.8)$$

where θ is a number satisfying

$$0 < \theta < 1. \qquad (B.9)$$

We may choose θ such that

$$0 \leq \varphi(\Delta v)/\Delta v \leq M, \qquad \text{(B.10)}$$

where M is some large but finite constant. This is possible because of our assumptions that $f'(v_0) < 1$ and that there is only one intersection (v_0, f_0). Eq. (6) becomes

$$\Delta v(t) = \theta \int_{0^-}^{\infty} k(t') \Delta v(t - t') \, dt' - \qquad \text{(B.11 a)}$$

$$- \int_{0^-}^{\infty} k(t') \varphi[\Delta v(t - t')] \, dt' + \Delta v_{\mathrm{h}}(t),$$

of which the Fourier transform is

$$V(\omega) = 2\pi \theta K(\omega) V(\omega) -$$
$$- 2\pi K(\omega) \Phi(\omega) + V_{\mathrm{h}}(\omega) \quad \text{(B.11 b)}$$

where V, K, Φ and V_{h} denote the Fourier transforms of $\Delta v(t)$, $k(t)$, $\varphi[\Delta v(t)]$ and $\Delta v_{\mathrm{h}}(t)$. This may be rearranged as

$$V(\omega) = - G(\omega) \Phi(\omega) + U_{\mathrm{h}}(\omega) \qquad \text{(B.12)}$$

where

$$G(\omega) = 2\pi K(\omega)/\{1 - 2\pi \theta K(\omega)\}, \qquad \text{(B.13)}$$

and

$$U_{\mathrm{h}} = V_{\mathrm{h}}/\{1 - 2\pi \theta K\}.$$

Now

$$\mathrm{Re}[G(0)] = 1/(1 - \theta) > 0$$

by eq. (B.1) and relation (B.9); so

$$\mathrm{Re}[G(\alpha)] > 0 \quad (0 \leq \alpha < \alpha_0) \qquad \text{(B.14)}$$

for some constant $\alpha_0 > 0$, since $G(\alpha)$ is a continuous function of α. Thus the Nyquist plot of $G(\alpha)$, i.e. the locus of $\{\mathrm{Re}[G(\alpha)], \mathrm{Im}[G(\alpha)]\}$ for $\alpha \geq 0$, lies in the right half of the G plane for $0 \leq \alpha < \alpha_0$. Moreover it lies below the real axis for all $\alpha > 0$, since from eq. (B.13) and then from relation (B.6) we have

$$|1 - 2\pi \theta K(\alpha)|^2 \mathrm{Im}[G(\alpha)] =$$
$$= \mathrm{Im}[2\pi K(\alpha)] \leq 0, \qquad \text{(B.15)}$$

with strict inequality unless $\alpha = 0$ or ∞.

If it can further be shown that the part of the Nyquist plot for $\alpha \geq \alpha_0$ lies on or to the right of some straight line L of finite, positive slope through the origin of the G plane, then this together with relations (B.10) and (B.15) will imply, by Popov's theorem ([26], eq. (10.19) and Fig. 10.4 b — a fortiori) that the system is stable in the sense that

$$(v, f) \to (v_0, f_0) \quad \text{as} \quad t \to \infty, \qquad \text{(B.16)}$$

no matter how large the disturbance imposed by the initial behaviour of $\Delta v_{\mathrm{h}}(t)$ before it reaches zero.

From eq. (B.13),

$$|1 - 2\pi \theta K(\alpha)|^2 \mathrm{Re}[G(\alpha)] =$$
$$= \mathrm{Re}[2\pi K(\alpha)] - \theta |2\pi K(\alpha)|^2 = \quad \text{(B.17)}$$
$$= \varepsilon + \mathrm{Re}[H(\alpha)] -$$
$$- \theta \{\varepsilon^2 + 2\varepsilon \mathrm{Re}[H(\alpha)] + |H(\alpha)|^2\} \quad \text{(B.18)}$$

by eq. (B.3). Now

$$\varepsilon - \theta \varepsilon^2 \geq 0 \quad \text{and} \quad |1 - 2\theta \varepsilon| \leq 1,$$

since $0 \leq \varepsilon < 1$ and $0 < \theta < 1$; and

$$|\mathrm{Re}[H(\alpha)]| \leq |H(\alpha)| \leq C \min(1, \alpha^{-1})$$

by relation (B.5). Therefore the expression (B.18)

$$\geq 0 - C \min(1, \alpha^{-1}) - \theta C^2 \min(1, \alpha^{-2}) \geq$$
$$\geq - S D \min(\alpha, \alpha^{-1}) \quad \text{when} \quad \alpha > \alpha_0,$$

for some positive constant S,

$$\geq S \mathrm{Im}[2\pi K(\alpha)]$$

by relation (B.6),

$$= S |1 - 2\pi \theta K(\alpha)|^2 \mathrm{Im}[G(\alpha)]$$

by eq. (B.15). Comparing this with the left-hand side of eq. (B.17) we see, noting relations (B.2) and (B.9), that

$$\mathrm{Re}[G(\alpha)] \geq S \mathrm{Im}[G(\alpha)] \qquad \text{(B.19)}$$

for $\alpha > \alpha_0$, which shows that the Nyquist plot for $\alpha > \alpha_0$ does indeed lie to the right of a straight line L through the origin with slope equal to S^{-1}; and stability follows.

(Received January 14th, 1978.)

References

[1] Helmholtz, H., On the sensations of tone. Dover, New York 1954 (English translation of the German edition of 1877), pp. 80—88.
[2] E.g. Krigar-Menzel, O. and Raps, A., Über Saitenschwingungen. Ann. Phys. Chem. (later Ann. Phys., Leipzig) 44 [1891], 623.
[3] Raman, C. V., On the mechanical theory of vibrations of bowed strings, etc. Indian Assoc. Cult. Sci. Bull. 15 [1918], 1.
[4] Schelleng, J. C., The physics of the bowed string. Scient. American, January [1974], 87.
[5] Friedlander, F. G., On the oscillations of the bowed string. Proc. Cambridge Phil. Soc. 49 [1953], 516.
[6] Keller, J. B., Bowing of violin strings. Comm. Pure Appl. Math. 6 [1953], 483.
[7] Schelleng, J. C., The bowed string and the player. J. Acoust. Soc. Amer. 53 [1973], 26². Schelleng's main results on bowing tolerance are given in his eqs. (1a) and (2), and in his footnote 10.

² Republished in Benchmark Papers in Acoustics (series editor, R. Bruce Lindsay), vol. 5: Musical acoustics, violin family (edited by C. M. Hutchins). Wiley-Halsted. New-York-London 1975.

[8] McIntyre, M. E., Schumacher, R. T. and Woodhouse, J., New results on the bowed string. Catgut Acoust. Soc. Newslett. 28 [1977], 27. See also: Aperiodicity in bowed-string motion (same authors). (Submitted to Acustica.)

[9] Cremer, L. and Lazarus, H., 6th ICA Congress, Tokyo, N. 2—3, 1968. See also Cremer, L., Der Einfluß des „Bogendrucks" auf die selbsterregten Schwingungen der gestrichenen Saite. Acustica 30 [1974], 119; an English translation of an earlier version appears in Catgut Acoust. Soc. Newslett. 18 [1972], 13[2] and 19 [1973], 21[2].

[10] Hancock, M., The mechanical impedance of violin strings. I and II. Catgut Acoust. Soc. Newslett. 23 [1975], 17 and 28 [1977], 14.

[11] Schumacher, R. T., Self-sustained oscillations of the bowed string. Acustica 43 [1979], 109.

[12] Anselone, P. M., Nonlinear integral equations. University of Wisconsin Press, Madison 1964.

[13] Benade, A. H., Fundamentals of musical acoustics. Oxford University Press, New York 1976. For a more recent review of work on wind instruments, see Fletcher, N. H., Air flow and sound generation in musical wind instruments. Ann. Rev. Fluid Mech. 11 [1979], 123.

[14] Cremer, L., Die Geige aus der Sicht des Physikers. Nachr. Akad. Wiss. Göttingen: II. Math. Phys. Kl. Nr. 12 [1971], 223[2].

[15] Schumacher, R. T., Some aspects of the bow. Catgut Acoust. Soc. Newslett. 24 [1975], 5.

[16] This method for imparting a transverse pluck of repeatable magnitude was suggested in Reinicke, W., Übertragungseigenschaften des Streichinstrumentenstegs. Catgut Acoust. Soc. Newslett. 19 [1973], 26[2]. The method does not excite torsional motion. This could perhaps be remedied by plucking the string with a fine thread glued to the surface of the string, with glue which came cleanly unstuck at a given tension.

[17] e.g. Truxal, J. G., Control system synthesis. McGraw-Hill, New York 1965, § 7.10.

[18] e.g. Ko, P. L. and Brockley, C. A., The measurement of friction and friction-induced vibration. Trans. Amer. Soc. Mech. Eng. Ser. F 92 [1970], 543.

[19] Rayleigh, J. W. S., The theory of sound. Dover, New York 1945.

[20] The series diverges at all rational points, and has no meaningful limit at irrational points. See for example: Hardy, G. H. and Littlewood, J. E., Some problems of Diophantine approximation I: The trigonometric series associated with the elliptic θ-functions. Acta Math. 37 [1914], 193. Theorem 2.30, for example, gives details of behaviour of a slightly simpler version of our series. Basically, the function represented by our series is well-behaved in the upper half of the complex plane, but behaves pathologically everywhere on the real axis, and cannot be analytically continued across the real axis.

[21] e.g. Graff, K. F., Wave motion in elastic solids. Oxford University Press, Oxford 1975, § 3.4.2.

[22] Input admittance curves at the bridges of a number of violins have been measured by Beldie, J. P., reported in Cremer, L., Darstellung des Geigenkörpers als ein Schwingungssystem mit vier Freiheitsgraden im tiefen Frequenzbereich. Nachr. Akad. Wiss. Göttingen: II. Math. Phys. Kl. Nr. 1, [1976], 1. Partially summarized in Beldie, J. P., Vibration and sound radiation of the violin at low frequencies. Catgut Acoust. Soc. Newslett. 22 [1974], 13. The complexity of these curves implies anharmonicity [13] as well as differential damping of string vibration modes. See also the results of Reinicke reported in [14].

[23] Schelleng, J. C., The violin as a circuit. J. Acoust. Soc. Amer. 35 [1963], 326[2].

[24] McIntyre, M. E. and Woodhouse, J., The acoustics of stringed musical instruments. Interdiscipl. Sci. Rev. 3 [1978], 157.

[25] Jeffreys, H. and Jeffreys, B. S., Methods of mathematical physics, 3rd ed. Cambridge University Press, Cambridge 1962, § 14.03.

[26] Hsu, J. C. and Meyer, A. U., Modern control principles and applications. McGraw-Hill, New York 1968, ch. 10 and Appendix C.

[27] Raman, C. V., On the wolf-note in bowed-string instruments. Phil. Mag. Ser. 6, 32 [1916], 391[2].

[28] Firth, I. M., The action of the cello at the wolf tone. Acustica 39 [1978], 252.